



RESEARCH PAPER



Searching for drug leads targeted to the hydrophobic cleft of dengue virus capsid protein

Liliane O. Ortlieb^{a,b}, Ícaro P. Caruso^{b,c} , Nathane C. Mebus-Antunes^d, Andrea T. Da Poian^d, Elaine da C. Petronilho^a, José Daniel Figueroa-Villar^a, Claudia J. Nascimento^e and Fabio C. L. Almeida^b 

^aDepartment of Chemistry, Military Institute of Engineering (IME), Rio de Janeiro, Brazil; ^bInstitute of Medical Biochemistry Leopoldo de Meis (IBqM) and National Center for Structural Biology and Bioimaging (CENABIO), Federal University of Rio de Janeiro (UFRJ), Rio de Janeiro, Brazil; ^cMultiusler Center for Biomolecular Innovation (CMIB) and Department of Physics, Institute of Biosciences, Letters and Exact Sciences (IBILCE), São Paulo State University (UNESP), São José do Rio Preto, Brazil; ^dInstitute of Medical Biochemistry Leopoldo de Meis (IBqM), Federal University of Rio de Janeiro (UFRJ), Rio de Janeiro, Brazil; ^eDepartment of Natural Sciences, Institute of Biosciences, Federal University of the State of Rio de Janeiro (UNIRIO), Rio de Janeiro, Brazil

ABSTRACT

We synthesised and screened 18 aromatic derivatives of guanylylhydrazones and oximes aromatic for their capacity to bind to dengue virus capsid protein (DENV C). The intended therapeutic target was the hydrophobic cleft of DENV C, which is a region responsible for its anchoring in lipid droplets in the infected cells. The inhibition of this process completely suppresses virus infectivity. Using NMR, we describe five compounds able to bind to the $\alpha 1$ - $\alpha 2$ interface in the hydrophobic cleft. Saturation transfer difference experiments showed that the aromatic protons of the ligands are important for the interaction with DENV C. Fluorescence binding isotherms indicated that the selected compounds bind at micromolar affinities, possibly leading to binding-induced conformational changes. NMR-derived docking calculations of ligands showed that they position similarly in the hydrophobic cleft. Cytotoxicity experiments and calculations of *in silico* drug properties suggest that these compounds may be promising candidates in the search for antivirals targeting DENV C.

ARTICLE HISTORY

Received 12 September 2021
Revised 2 November 2021
Accepted 3 November 2021

KEYWORDS

Dengue virus; DENV C; NMR; drug-ligand interaction; fluorescence



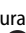

1. Introduction


The dengue virus (DENV) is a mosquito-borne virus that belongs to the *Flavivirus* genus, together with other important human pathogens, such as Zika, yellow fever, West Nile, and Japanese encephalitis viruses. The incidence of DENV is increasing over the years by the mosquito vector spreading, which can be associated with urbanisation, global warming, population growth, and an increasing number of international travels, together with a decrease in effective means for mosquito control¹. The disease caused by DENV may vary from a mild fever to life-threatening severe diseases, known as dengue haemorrhagic fever (DHF) and dengue shock syndrome (DSS), which are characterised by an increase in vascular endothelial permeability that leads to plasma leakage, and may evolve to a fatal hypovolemic shock².

DENV capsid protein (DENV C) forms a symmetric dimer in solution, presenting 8 intertwined α -helices (4 per subunit)³. DENV C has an essential role in the viral assembly. It is involved with the packaging of the viral genome forming the nucleocapsid (NC) core⁴. The protein is dominated by quaternary contacts involving two pairs of antiparallel helices ($\alpha 2$ - $\alpha 2'$ and $\alpha 4$ - $\alpha 4'$) that form most of the dimer interface. The $\alpha 4$ - $\alpha 4'$ exposed surface has the highest density of positive charges and it is the putative RNA binding site.

The $\alpha 2$ - $\alpha 2'$ is nonpolar and along with $\alpha 1$ and $\alpha 1'$ form a concave-shaped hydrophobic cleft, that interacts with the viral membrane. The dynamics, size, and orientation of $\alpha 1$ and $\alpha 1'$ regulate the exposure of the hydrophobic surface^{5,6}. Among flaviviruses, $\alpha 2$ - $\alpha 2'$ is the most conserved region of protein C, helping in the formation of a conserved hydrophobic surface (π -stacked Phe53/Phe53', Phe47, Leu54, and Leu57) and a conserved aromatic backbone (π -stacked Phe56/Phe84' and Phe56'/Phe84)⁶. Samsa and cols⁷ showed that DENV C associates with lipid droplets (LD) during viral replication, being this event essential to the virus assembly and infectivity. The interaction to LD involves the hydrophobic cleft of the DENV C and the conserved segment 14–23 of the intrinsically disordered N-terminal^{8,9}. Mutations in hydrophobic amino acid residues at the hydrophobic cleft completely abolished the virus infectivity, which makes it an important unexplored therapeutic target⁷.

Some antiviral compounds were identified as being able of inhibiting *in vitro* and *in vivo* DENV replication. Different targets were used in those studies, such as viral envelope (E) protein, inhibiting viral-induced membrane fusion¹⁰; NS2B-NS3, inhibiting viral protease activity¹¹; NS4B, possibly inhibiting its interaction with the viral NS3 helicase domain¹²; NS5 methyltransferase activity¹³ or RNA polymerase activity^{14,15}, inhibiting viral RNA synthesis;

CONTACT Fabio C. L. Almeida  falmeida@bioqmed.ufrj.br  Institute of Medical Biochemistry Leopoldo de Meis (IBqM) and National Center for Structural Biology and Bioimaging (CENABIO), Federal University of Rio de Janeiro (UFRJ), Rio de Janeiro, RJ, 21941-590, Brazil; Claudia J. Nascimento  claudia.nascimento@unirio.br  Department of Natural Sciences, Institute of Biosciences, Federal University of the State of Rio de Janeiro (UNIRIO), 22.290-240, Rio de Janeiro, Brazil

 Supplemental data for this article can be accessed [here](#).

© 2021 The Author(s). Published by Informa UK Limited, trading as Taylor & Francis Group.

This is an Open Access article distributed under the terms of the Creative Commons Attribution License (<http://creativecommons.org/licenses/by/4.0/>), which permits unrestricted use, distribution, and reproduction in any medium, provided the original work is properly cited.

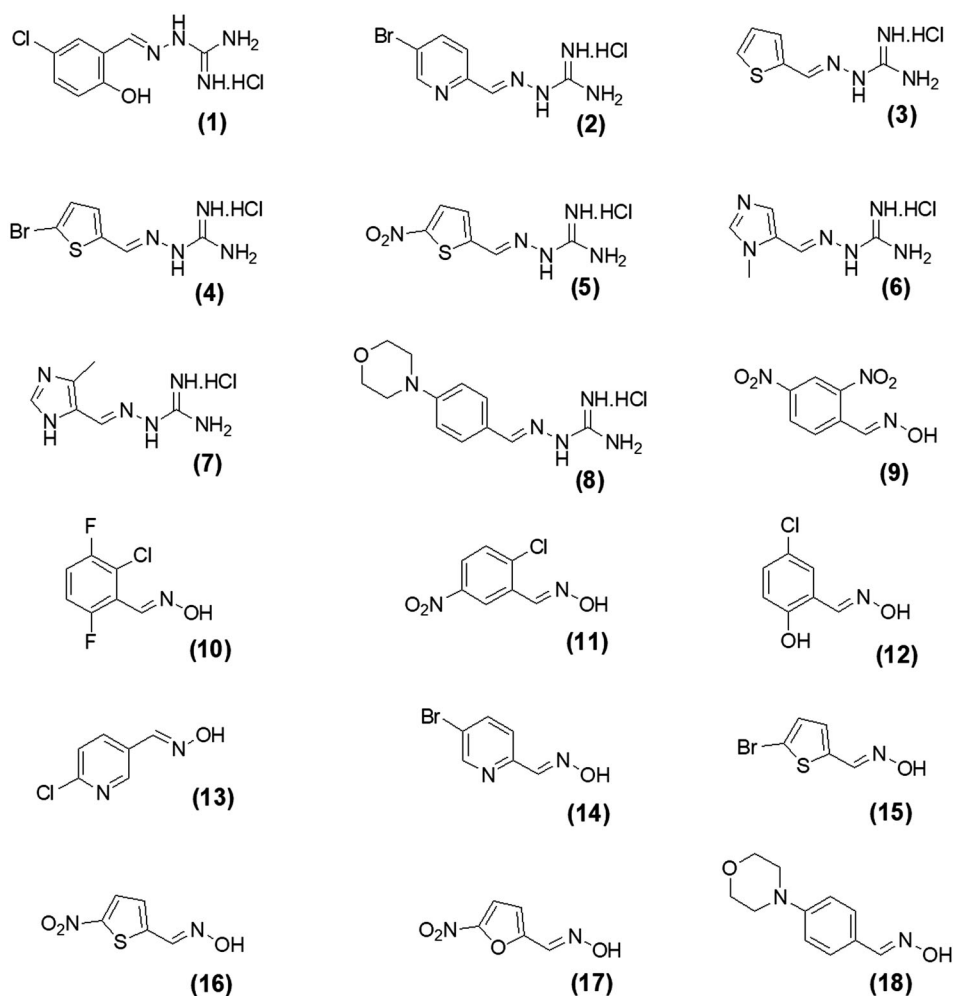


Figure 1. Organic compounds used in this work: (1) 5-chloro-salicylaldehyde-guanylhydrazone, (2) 5-bromo-pyridine-2-guanylhydrazone, (3) thiophene-2-guanylhydrazone, (4) 5-bromo-thiophene-2-guanylhydrazone, (5) 5-nitro-thiophene-2-guanylhydrazone, (6) 1-methyl-imidazole-5-guanylhydrazone, (7) 4-methyl-imidazole-5-guanylhydrazone, (8) 4-(4-morpholinyl)benzyl-guanylhydrazone, (9) 2,4-dinitro-benzoyloxime, (10) 2-chloro-3,6-difluoro-benzoyloxime, (11) 2-chloro-5-nitro-benzoyloxime, (12) 2-hydroxy-5-chloro-benzoyloxime, (13) 6-chloro-pyridine-3-oxime, (14) 5-bromo-pyridine-2-oxime, (15) 5-bromo-thiophene-2-oxime, (16) 5-nitro-thiophene-2-oxime, (17) 5-nitro-furfural-2-oxime, and (18) 4-(4-morphonyl)benzoyloxime.

and virus-specific RNA translation¹⁶. Regarding DENVC, the small compound ST-148 was identified as a ligand of C protein^{17,18}, with a proposed mechanism of capsid assembly inhibition through its binding to the protein hydrophobic cleft, leading to the formation of a kissing tetramer (dimer of dimers)¹⁹. Despite some of these ligands having shown valid antiviral activity against DENV replication, until now, to our knowledge, there are no interaction studies by NMR and no approved antiviral drug for the treatment of DENV infections.

In this work, we screened by NMR 18 aromatic compounds (Figure 1, derivatives of guanylhydrazones and oximes) for their capacity to bind DENVC. The intended target was the hydrophobic cleft. We selected 5 leads that bind to the hydrophobic cleft at the interface between $\alpha 1/\alpha 1'$ and $\alpha 2/\alpha 2'$. We used ligand-based NMR methods (saturation transfer difference, STD, and transverse relaxation, T_2) and protein-based ¹⁵N-HSQC for screenings. *In silico* calculations were also performed to rationalise the results. Structural models of the protein-ligand complexes generated by NMR-derived molecular docking showed that the selected compounds could bind to the two symmetric pockets in the hydrophobic cleft. Pharmacokinetics analyses showed the tested compounds are promising drugs, with low cytotoxic effects on two different cell lines (Huh7 and A549). We successfully

addressed the hydrophobic cleft of DENVC as a structural target for the development of potential antiviral compounds.

2. Materials and methods

2.1. Compounds selection

The selection of the compounds used in this work (Figure 1) was based on the fact that aromatic and amphipathic compounds are expected to interact with the nonpolar exposed residues and the aromatic backbone in DENVC hydrophobic cleft. In addition, it has been taken into account fact that derivatives of guanylhydrazones and oximes are widely studied due to their broad biological activity, as antitumor^{20,21}, antibacterial^{22,23}, antifungal^{24,25}, antiviral^{26,27}, antiprotozoal^{28,29}, and anti-inflammatory^{30,31} drugs.

2.2. Synthesis and characterisation of the organic compounds

All reagents were purchased from Sigma-Aldrich (Brazil) and the solvents from VETEC (Brazil), used without further purification. Reactions were monitored by TLC using DC Alufolien Kieselgel 60 F254 (Merck, Darmstadt, Germany). Melting points (MP) were

determined on a Melt-Temp II with a previously calibrated thermometer. Infra-red spectra (IR) were obtained on a Shimadzu Prestige 21. For the characterisation of compounds, all NMR experiments (^1H NMR, ^{13}C NMR, ATP, gHSQC, gHMBC) were performed at 298 K on a 14.1 T Premium COMPACTTM (600 MHz for proton, software VNMRJ version 3.2) spectrometer using a 5 mm NMR probe and dimethylsulfoxide- d_6 (DMSO- d_6) as solvent and reference. The data of yield, melting point, IR and NMR spectra (Figures S1–S54), and spectral assignment are available in the Supplementary Information.

2.2.1. General procedure for the synthesis of guanilhydrazones (1–8):

Aminoguanidine hydrochloride (1.2 mmols) dissolved in 20 ml of 95% ethanol, the corresponding aldehyde (1 mmol) and 2 drops of HCl (0.6 M) were placed in a round bottom flask. The solution was kept under reflux and stirring. The solid obtained after eliminating the solvent under vacuum was solubilised in distilled water and extracted with dichloromethane (5×20 ml). The product was recrystallized from ethanol³².

2.2.2. General procedure for the synthesis of oximes (9–18):

Hydroxylamine hydrochloride (4 mmols) dissolved in a mixture of 10 ml of ethanol and 3 ml of water was placed in a round bottom flask. The corresponding aldehyde (2 mmols) was added to the solution, which was kept under stirring. The solid obtained after eliminating the solvent under vacuum was washed with distilled cool water. The oximes were recrystallized from ethanol or methanol³². The compounds **1**, **3**, **12**, **15**, **16**, and **17** were synthesised as previously reported^{33–38}. The synthesis routes were the same as published, optimising the quantities of the reagents and time of reaction.

2.3. DENE expression and purification

DENVC from serotype 2, strain New Guinea, was expressed in *Escherichia coli* BL21(DE3)plysS cells with pET3a (Novagen) expression plasmid in M9 minimal medium, as previously described^{3,39}. For expression of the ^{15}N -labelled protein, the minimal medium containing $^{15}\text{NH}_4\text{Cl}$ $1 \text{ g} \cdot \text{L}^{-1}$ (Sigma Aldrich) was used. The DENVC was purified using a heparin column (GE Healthcare LifeSciences) at 5 ml/min flow rate and the bound protein was eluted with an increasing NaCl concentration gradient (0.5–2.0 M). The fractions containing the DENVC were confirmed by 15% SDS-PAGE. The DENVC was dialysed against phosphate-buffered saline (PBS) with a Centricon instrument (Millipore) and stored at -20°C .

2.4. Ligand-protein interaction studies by NMR

Stock solutions of compounds **1–8** were prepared in H_2O . Due to the low solubility in water, stock solutions of compounds **9–18** were prepared in DMSO- d_6 . For the NMR experiments, samples were prepared using the necessary amount of stock solution in 55 mM PBS, 200 mM NaCl, 2 mM EDTA, 10% (v/v) D_2O (Cambridge Isotope Laboratories) as buffer solution at pH 6.0.

All experiments were acquired using the samples in the presence and absence of DENVC, with the final concentration of $10 \mu\text{M}$ for the protein and 1 mM for ligands (100-fold excess). For compounds **9–18**, the final concentration of DMSO- d_6 was 5% (v/v). All experiments were performed at 308 K, using a 5 mm NMR

probe. Spectral data were processed with Topspin 2.1 (Biospin; Bruker).

Initially, the saturation-transfer difference (STD) experiments were performed in pools of 4 or 5 compounds, using STDdiff pulse sequence, 8 scans, 4 dummy scans, off-resonance irradiation at -6000 Hz, and on-resonance irradiation at 124.7, 746, and 2688 Hz, on a Bruker Avance DRX 400 MHz (Bruker Biospin, Germany). For those compounds that showed interaction, new STD spectra were acquired for each compound separately under the same previously described conditions on a Bruker Ascend 500 MHz spectrometer (Bruker Biospin, Germany).

The ^1H NMR chemical shift variations were recorded using zgesgp pulse sequence (excitation sculpting for water suppression)⁴⁰ with 32 scans and 8 dummy scans. DOSY experiments were acquired using bipolar gradients (stebpgp pulse sequence) with 128 scans, 4 dummy scans, 20 ms of diffusion time (big delta), and 10 ms of gradient pulse (little delta). Both experiments were performed on a Bruker Avance DRX 400 MHz (Bruker Biospin, Germany).

The diffusion coefficients calculations were calculated from the adjustment of curves using the following fitting equation, where A and A_0 are the areas of the NMR signal in the presence and absence of external gradient pulses, respectively; D is the diffusion coefficient; γ is the gyromagnetic ratio of the observed nucleus; g is the gradient strength; Δ is the diffusion time; δ is the length of the gradient.

$$A = A_0 \exp \left[-D \cdot \gamma^2 \cdot g^2 \cdot \delta^2 \cdot \left(\Delta - \frac{\delta}{3} \right) \right] \quad (1)$$

Relaxation times were acquired on a Bruker Ascend 500 MHz spectrometer (Bruker Biospin, Germany) and performed in triplicate with a recycle delay of 10 s. T_1 relaxation time was measured using the inversion recovery pulse sequence and T_2 relaxation time by Carr-Purcell-Meiboom-Gill (CPMG) pulse sequence.

In addition, protein-ligand studies for determining the binding sites of the protein were performed only for those ligands that showed interaction by STD. HSQC ^1H - ^{15}N spectra were acquired using the uniformly labelled ^{15}N DENVC. The experiments were performed in the presence and absence of the ligands. For the first titration point, a $200 \mu\text{M}$ DENVC solution was used. For the next four titration points, it was used a molar excess of the ligands: 1, 3, 6, and 9 relative to the protein. Samples were prepared in PBS buffer (55 mM $\text{NaH}_2\text{PO}_4/\text{Na}_2\text{HPO}_4$, 200 mM NaCl, 5 mM EDTA, pH 6.0) with 10% (v/v) D_2O (Cambridge Isotope Laboratories), and 5% (v/v) DMSO- d_6 (Cambridge Isotope Laboratories). Spectra were acquired on a Bruker Avance III 18.6 Tesla (800 MHz for hydrogen) spectrometer with a 5 mm probe at 308 K using the hsqctf3gpsi pulse sequence, water suppression by water flip back and gradients^{41–44}, 8 scans, 16 dummy scans, 1024×256 dot spectral window. The experiments were processed using the CcpNmr Analysis software⁴⁵ and were assigned according to NMR data (PDB ID code 1R6R)⁴⁶ obtained from the Biological Magnetic Resonance Data Bank (BMRB)⁴⁷.

2.5. Fluorescence analysis

Fluorescence measurements were taken in a Varian Cary Eclipse Fluorescence Spectrophotometer at 308 K. One scan was performed on a $10 \mu\text{M}$ DENVC sample in PBS buffer using an excitation wavelength of 280 nm and emission detected from 300 to 420 nm with slits set to 5 nm (excitation) and 10 nm (emission). Stock solutions of compounds **1** and **4** were prepared in H_2O and for compounds **12**, **15**, and **16**, due to their low solubility in

water, in DMSO- d_6 . The protein sample was titrated by adding aliquots of the ligand stock solution in different concentrations, according to each protocol, as described in Figure 2.

A total of 10 titration points was acquired for each inhibitor, compound **1**: apo, 3.33, 6.67, 10, 20, 30, 40, 60, 80, and 100 μM ; compound **4**: apo, 10, 20, 30, 60, 90, 120, 150, 180, and 210 μM ; compound **12**: apo, 40, 80, 120, 160, 200, 280, 360, 520, and 680 μM ; compound **15**: apo, 10, 30, 50, 70, 90, 110, 130, 150, and

190 μM ; and compound **16**: apo, 3, 9, 15, 21, 27, 36, 45, 54, and 63 μM .

Before each measurement, the samples were placed to reach thermal equilibrium for 10 min. Each experiment was performed in triplicate and the solvent (blank) with each compound was subtracted from the mean of three means of three replicate samples. The values of maximum emission wavelength (λ_{max}) were used to build the binding isotherms for the DENVC/selected compound

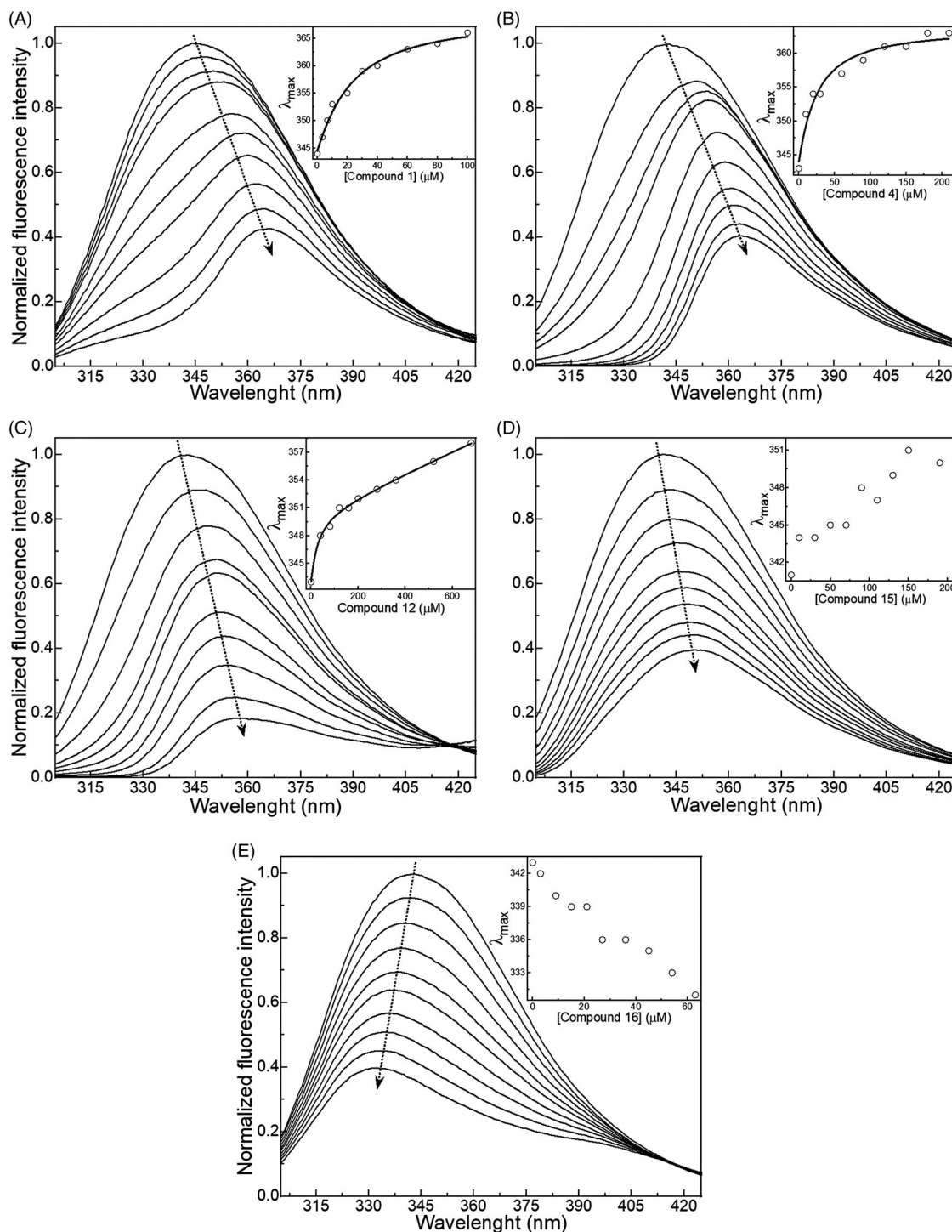


Figure 2. Effect of intrinsic fluorescence on the relative intensity of the signal of DENVC (10 μM) obtained by titration of compounds with excitation at 280 nm and scanning emission between 305 and 425 nm in the absence and presence of compound: (A) **1**, (B) **4**, (C) **12**, (D) **15**, and (E) **16**. The insets show the change in the maximum emission wavelength (λ_{max} , open circle) as a function of the selected compound concentration. The black line in the insets denotes the better fitting to the experimental data.

interactions. The program Origin 2021 was employed to fit the following equation to the experimental data⁴⁸:

$$\lambda_{max} = \lambda_{max}^0 + \left(\frac{\lambda_{max}^{sat} - \lambda_{max}^0}{2 \cdot [P_T]} \right) \left[(K_d + [L_T] + [P_T]) - \sqrt{(K_d + [L_T] + [P_T])^2 - 4 \cdot [L_T] \cdot [P_T]} \right] \quad (2)$$

where λ_{max}^0 and λ_{max}^{sat} are the initial and saturation maximum emission wavelength, respectively, K_d is the dissociation constant, $[L_T]$ is the total concentration of the selected compound, and $[P_T]$ is the total concentration of the DENVC. For compound **12**, it was added a linear contribution to Equation (2) to perform the fitting.

2.6. Pharmacokinetic and toxicological properties

In silico pharmacokinetic and toxicological properties (molecular weight (g/mol), relative polar surface area (PSA) (Å), lipophilicity (c-LogP), water solubility (c-LogS), donor sites (nOHNH), hydrogen bonding acceptors (nOH), number of rotatable bonds, and toxicity), using DataWarrior software⁴⁹, were calculated for the five compounds that showed interaction by STD-NMR experiment.

2.7. Molecular docking

The DENVC structure used for the computational simulations was downloaded from Protein Data Bank (PDB) under access code 1R6R⁴⁶. The molecular structures of the compounds were obtained by structural optimisation calculations from the semi-empirical PM6 method using the Gaussian 09 program⁵⁰. DENVC and compounds were prepared using AutoDockTools program⁵¹ for molecular docking simulations, merging non-polar hydrogen atoms, and adding atom types. The rigid root of the compounds was generated automatically, setting all possible rotatable bonds defined as active by torsions. The molecular docking calculations were performed in triplicate by using AutoDock Vina⁵², applying a total of 8 exhaustiveness. The coordinates of the centre of the conformational search box were defined to enrol the whole hydrophobic cleft ($\alpha 1/\alpha 1'$ and $\alpha 2/\alpha 2'$) in DENVC since ¹H-¹⁵N HSQC experiments indicate that all compounds bind to this protein region. The box dimensions were 40 × 30 × 20 Å on the three coordinate axes. Following docking calculations, the lowest energy structural models of DENVC/compound complexes were analysed by PLIP webserver⁵³ for characterising the protein/ligand non-covalent interactions, such as hydrophobic contacts, hydrogen bond, π -cation interaction, and halogen bonds. Structural conformation of the constructed models was displayed using PyMOL⁵⁴.

2.8. Cytotoxicity assay

Stock solutions (200 mM) of the lyophilised form of the compounds **1**, **4**, **12**, **15**, and **16** were prepared in dimethyl sulfoxide (DMSO) and then stored at -20 °C. For the experimental procedures, the stock solutions were diluted in PBS keeping a final concentration of 5% DMSO. Each solution was used to treat the cells at the established concentrations. Human hepatocarcinoma cell line (Huh7) and human epithelial lung cells (A549) were cultured in Dulbecco's modified Eagle's medium (DMEM), supplemented with 10% foetal bovine serum (FBS) (Invitrogen, USA), 100 U/mL penicillin, 100 g/mL streptomycin, 0.22% sodium bicarbonate, and 0.2% HEPES (pH 7.4), in a CO₂ humid incubation chamber, at 37 °C. The cytotoxicity of compounds was evaluated *in vitro* using

a 3-(4,5-dimethylthiazol-2-yl)-2,5-diphenyl tetrazolium bromide (MTT) (USB, Ohio, USA) assay. Monolayers with 6 × 10⁴ cells per well of the Huh7 and A549 cell lines were prepared in, 48-well, cell culture plates. The cells were treated with increasing concentrations of compounds and the times of 24 and 48 h after treatment were analysed. After this time, the cells were incubated for 40 min with 0.5 mg/mL of MTT at 37 °C. Next, the solution was removed and precipitated formazan was diluted in isopropyl alcohol with 40 mM HCl. Absorbance was measured for each well at 570 nm (compounds-treated and control) and 650 nm (background). The percentage of cell viability was calculated as follows: 100% × (absorbance of treated cells) - (background)/(absorbance of untreated cells) - (background).

Statistical analyses were performed using GraphPad Prism 8.0.2 (GraphPad Software, Inc.). Results are presented as means ± standard errors (SEM) and were compared by two-way analysis of variance (ANOVA) and Dunnett's multiple comparisons test *p* values of ≤ 0.05 were considered significant.

3. Results and discussion

3.1. Synthesis and characterisation of the organic compounds

Eighteen compounds were used in this study, 8 aromatic guanylhydrazones and 10 aromatic oximes (Figure 1). We chose aromatic and amphipathic compounds to target the interaction with the hydrophobic cleft ($\alpha 1/\alpha 1'$ and $\alpha 2/\alpha 2'$) in DENVC. We expect the aromatic compounds to interact with the nonpolar exposed surface and with the aromatic backbone at the hydrophobic cleft.

Compounds **1–8** were synthesised in the one-step reaction between the correspondent aldehydes and aminoguanidine hydrochloride, using ethanol (95%) as the solvent, HCl as the catalyst, and heating under reflux for 3–23 h, generating monocationic compounds obtained in 70–97% yields. The mechanism for those reactions is based on the nucleophilic attack of the -NH₂ group of aminoguanidine to the -C=O group of the aldehyde, followed by the loss of molecule water and the formation of a double bond, leading to the corresponding guanylhydrazone (Supplementary Information, Scheme S1).

The oximes **9–18** were prepared by the reaction of hydroxylamine hydrochloride with the corresponding aldehydes, using ethanol (95%) and distilled water as solvents^{26,55,56}. After stirring, the product was vacuum filtered and washed with cold distilled water, leading to compounds obtained in 50–98% yields. The time of stirring (1–36 h) and the yield for each compound is described in Supplementary Material with the spectral assignment data. The mechanism for forming oximes is similar to that of guanylhydrazones, based on the nucleophilic attack of the -NH₂ group of hydroxylamine to the -C=O group of the aldehyde, followed by loss of water and formation of the double bond (Supplementary Information, Scheme S2). Compounds **2**, **4**, **5–11**, **13**, **14**, and **18** are new unpublished agents. Although compounds **1**, **3**, **12**, **15**, **16**, and **17** have already been reported in the literature, they have never been tested as DENVC inhibitors. All compounds were characterised by infra-red spectroscopy (IR) and NMR (Supplementary Information, Figures S1–S54).

3.2. Ligand-protein interaction studies

To identify the compounds able to bind DENVC, we performed NMR STD experiments. We made pools of 4–5 compounds. The pools were divided according to the observed proton NMR chemical shifts, avoiding overlaps of the signals of the different

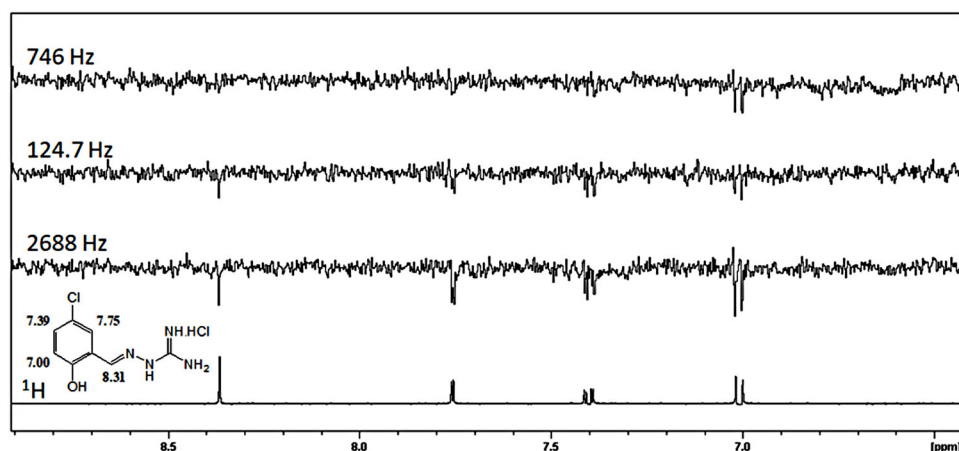


Figure 3. STD spectrum of 1 mM of compound **1** and 10 μ M of DENVC in PBS buffer H₂O/D₂O (90%/10%) at different frequencies of irradiation (746, 124.7, and 2688 Hz). At the bottom, the reference ¹H-NMR spectrum of the compound.

Table 1. T_1 and T_2 values for 1 mM of compounds **1**, **4**, **12**, **15**, and **16** in the absence and the presence of 10 μ M of DENVC.

Compound	Hydrogen number	T_1 ligand (s)	T_1 ligand+protein (s)	T_2 ligand (ms)	T_2 ligand+protein (ms)
(1)	1	1.11	1.69	390.46	441.42
	2	3.09	3.14	602.32	416.99
	3	3.30	2.94	639.53	431.33
	4	1.84	2.39	545.66	471.80
(4)	1	2.58	2.13	752.86	501.96
	2	4.60	3.96	1293.60	559.59
	3	3.23	2.84	1062.49	505.95
(12)	1	3.39	3.36	1186.65	840.66
	2	3.46	3.44	1298.42	787.54
	3	4.26	3.84	1350.42	758.63
	4	3.80	3.76	1312.56	863.21
(15)	1	4.70	4.12	701.83	655.41
	2	4.19	3.47	1120.43	639.71
	3	4.70	4.12	1171.62	654.88
(16)	1	5.58	5.82	896.06	1040.06
	2	6.62	5.82	1982.16	1623.02
	3	4.68	4.17	1597.08	1347.14

compounds (Figures S55–S58). The STD spectra for pools 1–4 (Figures S59–S62) showed that compounds **1**, **4**, **11**, **12**, **15**, and **16** binds to DENVC. For these selected ligands, we ran STD experiments for each compound. Compound **11** showed an STD weak signal near the noise (Figure S61) and thus it was not selected for further analysis. The analysis of the compound **1** STD spectrum revealed that all hydrogens are involved in the binding site of DENVC (Figure 3). Similar results were observed for compounds **4**, **12**, **15**, and **16** (Figures S63–S66).

To investigate the intermolecular interaction between DENVC and the selected compounds, we also analysed relaxation parameters⁵⁷. We measured proton relaxation times T_1 and T_2 for the selected compounds in the presence and absence of DENVC (Table 1). Changes in T_1 and T_2 values for compounds **1**, **4**, **12**, **15**, and **16** after the addition of the protein corroborate the STD experiments, showing that all compounds interact with DENVC. As expected for binding, T_2 of all compounds increased in the

Table 2. Diffusion coefficient (D) for 1 mM of compounds **1**, **4**, **12**, **15**, and **16** in the presence and absence of 10 μ M of DENVC.

Compound	D_{ligand} (10^{-10} m ² /s)	$D_{\text{ligand+protein}}$ (10^{-10} m ² /s)
1	7.07	6.26
4	7.30	6.95
12	7.81	7.17
15	7.78	7.22
16	7.98	7.80

presence of the protein, with the exception of hydrogen 1 of compounds **1** and **16**. This change could be a result of the presence of conformational exchange at this site in the free ligand that is reduced upon binding. Interestingly, it occurred in the same site for both compounds. The aromatic hydrogens of all compounds presented major T_2 changes, suggesting the aromaticity of these compounds is important for the interaction.

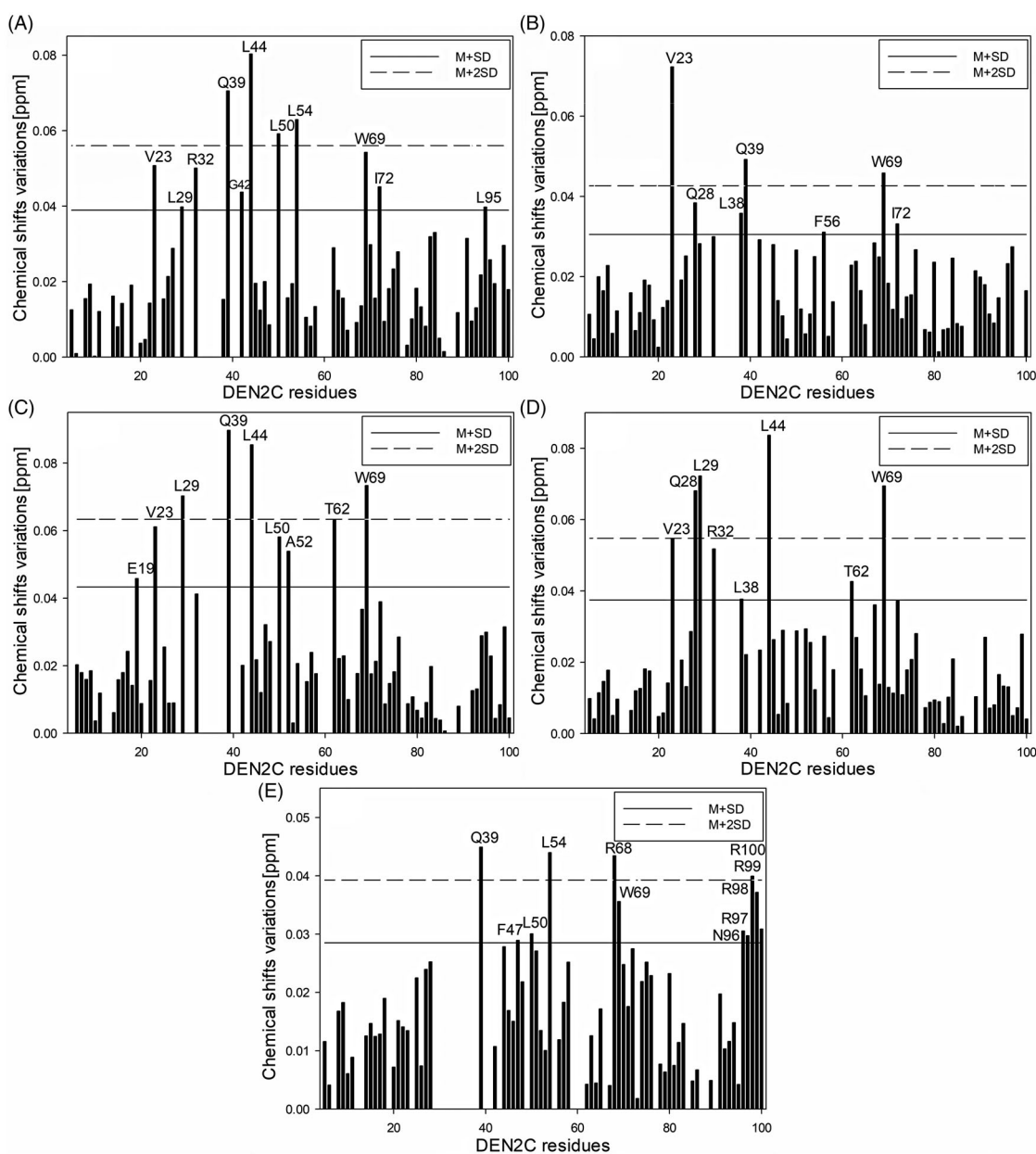


Figure 4. DENVC (200 μ M) chemical shift perturbations (CSP) mapped by HSQC ^1H - ^{15}N in the absence and presence of 1.8 mM of (A) compound **1**, (B) **4**, (C) **12**, (D) **15**, and (E) **16**. The solid line denotes the average CSP value (M) for all residues plus the standard deviation (SD), and the dashed line indicates the average plus twice standard deviation (2SD).

We also measured the translational diffusion coefficient in the presence and absence of DENVC (Table 2). We observed a decrease in the diffusion coefficient for all compounds in the presence of the protein. Accordingly, such a decrease is expected when a small molecule binds to a high molecular weight biomolecule like a protein⁵⁸.

To identify the DENVC residues involved in the binding, we mapped the changes in the signal intensity and chemical shift perturbation (CSP) for all residues by ^1H - ^{15}N -HSQC experiments in the presence and absence of the selected compounds (**1**, **4**, **12**, **15**, and **16**) (Figures 4 and S67). The residues showing the highest changes according to the average plus one standard deviation (M + SD) and the average plus two standard deviations (M + 2SD) (Table S1) were selected and represented along with the three-dimensional structure of the DENVC (Figure 5). When we mapped the CSP values and changes in intensity in the protein structure, we observed perturbations at α 1, α 2, and α 3 helices, indicating

that the compounds interact in the hydrophobic cleft, the targeted region.

The residues identified by ^1H - ^{15}N -HSQC experiments were: for compound **1**, V23, L29, and R32 in α 1, Q39, G42, and L44 in the α 1- α 2 loop, L50 and L54 in α 2, R68 and W69 in α 3, I72 in the α 3- α 4 loop, L95 in α 4, and R99 in the C-terminal region; for compound **4**, V23, Q28, and L29 in α 1, L38, Q39, and L44 in the α 1- α 2 loop, L50, L54, and F56 in α 2, R68 and W69 in α 3, and I72 in the α 3- α 4 loop; for compound **12**, E19 in the N-terminal region, V23, Q27, L29, and R32 in α 1, M37, Q39, G42, and L44 in the α 1- α 2 loop, L50, A52, and L54 in α 2, T62 in the α 2- α 3 loop, and R68 and W69 in α 3; for compound **15**, V23, Q27, Q28, L29, and R32 in α 1, L38 and L44 in the loop α 1- α 2, L50 and V51 in α 2, T62 in the α 2- α 3 loop, R68 and W69 in α 3, L95 in α 4, and R99 in the C-terminal region; and for compound **16**, S24, V26, and Q27 in α 1, Q39 and F47 in the α 1- α 2 loop, L50, A52, and L54 in α 2, R68 and W69 in α 3, F84 and N96 in α 4, and R97, R98, R99, and R100 in the

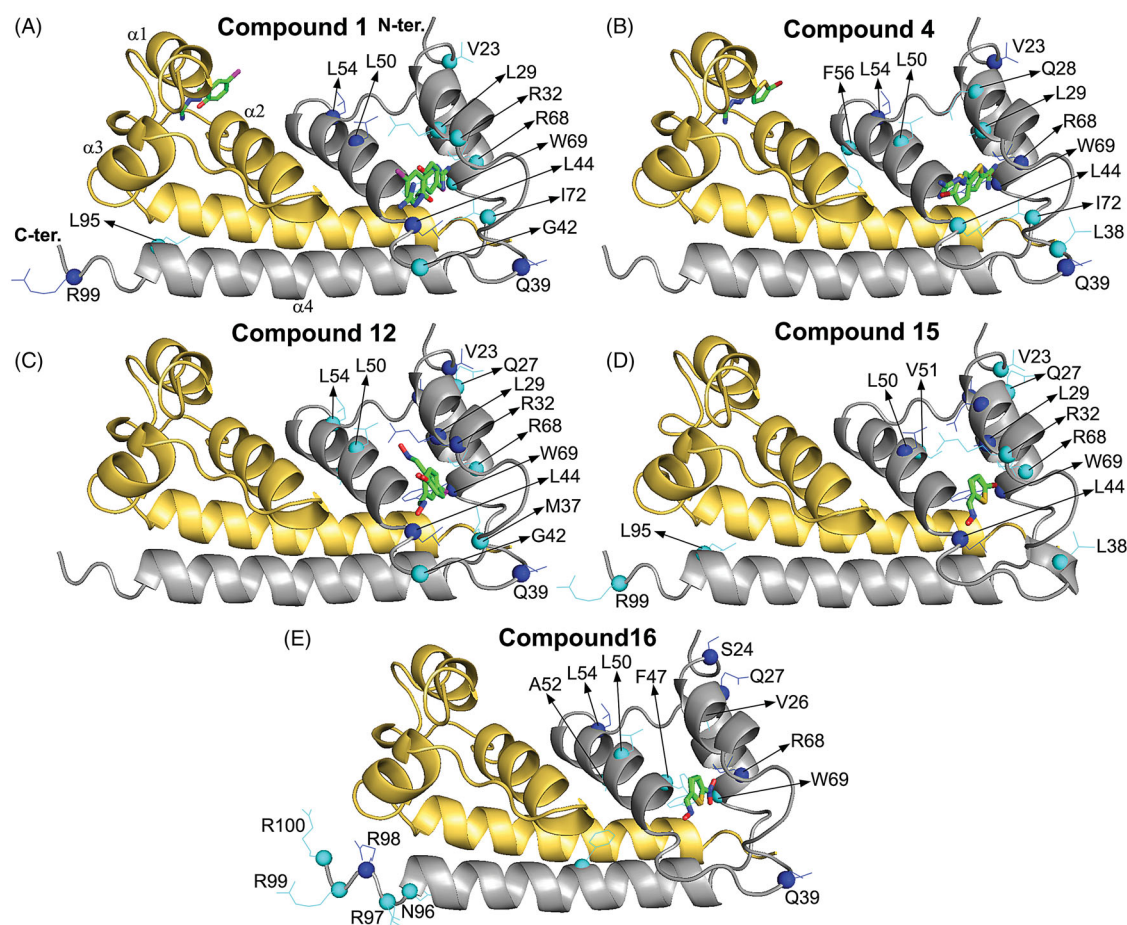


Figure 5. Analysis of the molecular docking results for the structural model of the complex of DENVC with compounds 1 (A), 4 (B), 12 (C), 15 (D), and 16 (E). All compounds are in the symmetric pockets of the hydrophobic cleft in DENVC. The protein is shown as a cartoon model with the monomers coloured in grey for chain A and golden yellow for chain B. The secondary structures of α -helix of the chain B are indicated as $\alpha 1$, $\alpha 2$, $\alpha 3$, and $\alpha 4$. The compounds are denoted as a stick model with carbon, oxygen, nitrogen, sulphur, chlorine, and bromine coloured in green, red, blue, yellow, magenta, and dark red, respectively. The residues with changes in chemical shift (CSP) and intensity higher than $M + SD$ and $M + 2SD$ are denoted as cyan and blue lines/spheres, respectively.

C-terminal region. Residues L50 in $\alpha 2$, the core of the hydrophobic cleft, and R68 and W69 in $\alpha 3$ stand out since they are perturbed in all compounds. Compound **16** promoted singular changes in CSP values of the C-terminal residues. It is worth mentioning that W69, with the side chain in the $\alpha 2$ – $\alpha 3$ interface, can be used as a fluorescent probe for investigating the DENVC/selected compound interaction.

We used the intrinsic tryptophan fluorescence of DENVC to measure the binding affinity of each of the selected compounds. All compounds led to fluorescence quenching as a consequence of protein binding. For compounds **1**, **4**, **12**, and **15**, the binding resulted in a redshift of the tryptophan fluorescence spectra, indicating the exposure of W69 to a more polar environment. Conversely, for compound **16**, the binding led to a blue shift in the spectrum, meaning that, in this case, W69 is buried in a more hydrophobic environment⁵⁹ (Figure 2). Interestingly, compound **16** showed significant CSP values in the C-terminal region (Figure 5(E)). The results suggest a specific interaction of these compounds with DENVC, inducing a conformational change in the protein. The dissociation constants (K_d) were calculated using the change in the maximum emission wavelength (λ_{max}) as a function of the ligand concentration (inset in Figure 2). Compounds **1**, **4**, and **12** presented a hyperbolic binding isotherm, displaying K_d of 18 ± 4 , 20 ± 7 , and $23 \pm 8 \mu\text{M}$, respectively. Compounds **15** and **16** displayed an almost linear isotherm in the measured

concentration ranges, probably because they presented affinities in the millimolar range.

The ^1H - ^{15}N HSQC experiments indicated that all selected compounds bind to the hydrophobic cleft in DENVC. These experimental results drove the docking calculation of the compounds in the protein binding site. Figure 6 shows the structural models of the DENVC/compounds complexes determined from the docking calculations. The docking poses of the compounds correspond to the lowest energy conformers for the triplicate calculations. It is possible to observe in Figure 5 that the compounds interacted in the two symmetric pockets of the hydrophobic cleft in DENVC. These symmetric pockets are formed by the $\alpha 1$ – $\alpha 2$ loop and $\alpha 3$ on both chains of the dimer. An analysis of the non-covalent interactions involved in the structural models revealed the occurrence of hydrophobic contacts and hydrogen bonds in all DENVC/compound complexes, while π -cation interactions appeared exclusively to the compounds **1** and **4** and halogen bonds to the compound **15** (Table S2–S6). In at least two of the three replicas, compound **1** presented hydrophobic interactions with P43 and L46 and formed hydrogen bonds with L29, R41, and L44 (Table S2). The same hydrophobic contacts were observed for compound **4** (Table S3), but the hydrogen bond was only recurrent with L29. Compound **12** showed the highest number of hydrophobic interactions, being formed with L29, R32, F33, L44, L46, and F47, while only one hydrogen bond was formed with R41 (Table S4).

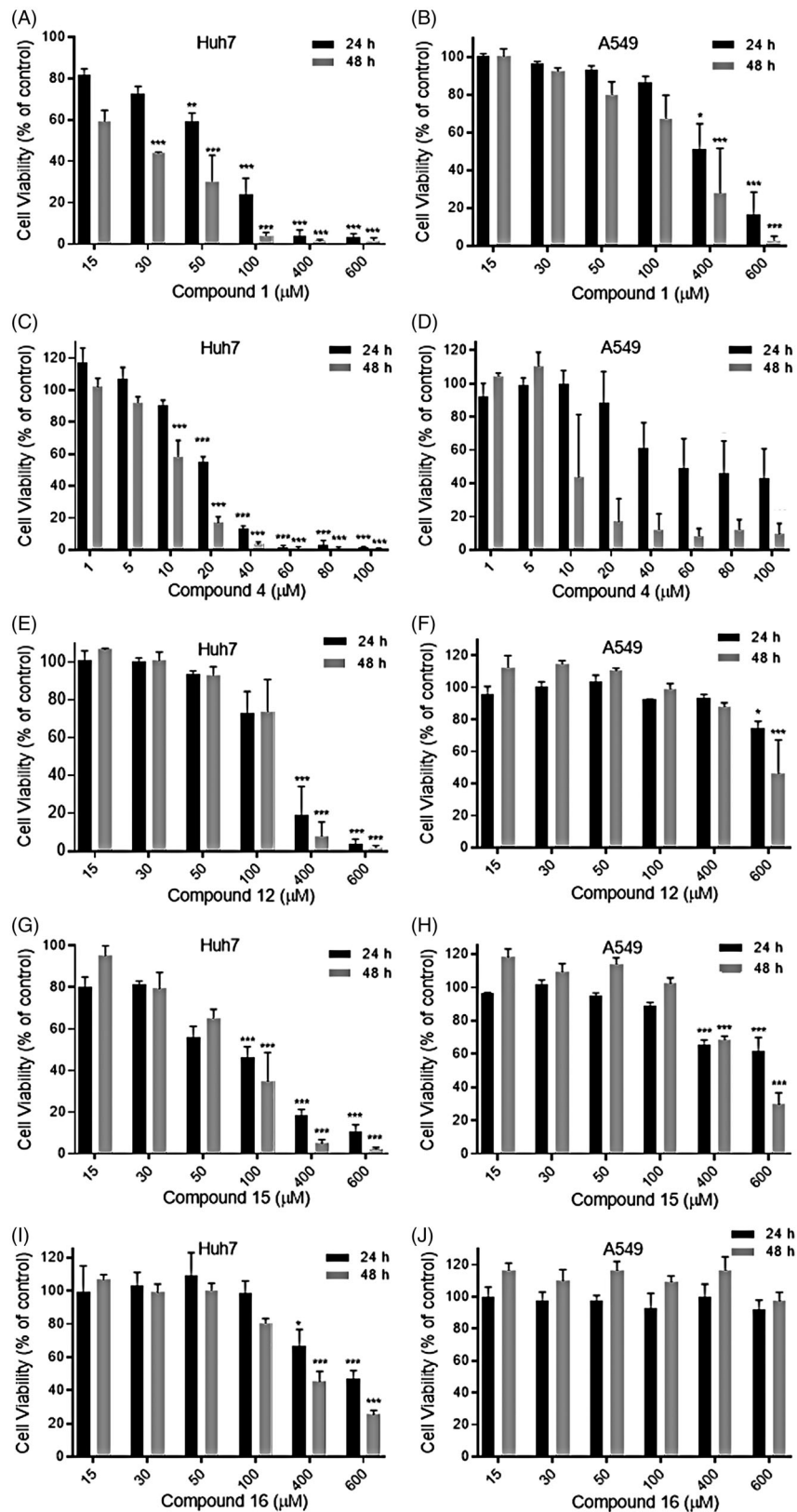


Figure 6. Cytotoxicity of the studied compounds in Huh7 and A549 cells by the MTT assay. The schematic figures of each panel illustrate the cell viability after treatment with increasing concentrations of the respective compounds (1, 4, 12, 15, and 16) in Huh7 (A, C, E, G, and I) and A549 (B, D, F, H, and J) cells, after 24 (black column) and 48 h (grey column). The results are presented as a percentage of the cell viability of the treated cells in relation to the untreated cell maintained in DMEM medium with 0.5% DMSO. Data are represented as mean \pm SEM of the results of at least three independent experiments. For statistical analysis, each treated condition was compared with the untreated control at the respective times. Asterisks indicate significant differences between untreated cells and treated cells as follows: * $P \leq 0.05$; ** $P \leq 0.01$; *** $P \leq 0.0001$.

Table 3. *In silico* pharmacokinetic parameters and toxicological properties of compounds.

Compound	MW	PSA	cLogP	cLogS	nOH	nOHNH	RBs	Toxicological
1	249.10	94.49	1.00	-2.43	4	5	2	NT, NM, NR, NI
4	283.58	102.50	1.53	-2.86	3	4	2	NT, NM, NR, NI
12	171.58	52.82	2.47	-2.76	2	3	1	NT, NM, NR, NI
15	206.06	60.83	3.01	-3.18	1	2	1	NT, NM, NR, NI
16	173.17	106.65	1.35	-2.94	1	5	2	NT, NM, NR, NI

MW: molecular weight (g/mol); PSA: polar surface area in Å²; cLogP: bipartition coefficient; cLogS: solubility; nOH: hydrogen bonding donors; nOHNH: hydrogen bonding acceptors; RBs: rotatable bonds; NT: non-tumorigenic; NM: non-mutagenic; NR: non-reproductive effective; NI: non-irritant.

Compounds **15** and **16** established hydrogen bonds with R41 and L44 in two of three docking runs (Tables S5 and S6). The hydrophobic contacts were remarkably similar for these compounds, being formed with L29, R32, and L46, except F47 that was observed only for compound **16**. It is possible to see that R41 and L46 are important residues for the binding of all compounds in the symmetric pockets of DENVC hydrophobic cleft, the former involved in hydrogen bonds, and the last in hydrophobic interaction. It is worth mentioning that R41 also is the main residue responsible for the formation of π -cation interactions with compounds **1** and **4** (Tables S2 and S3). Interestingly, the halogen bond is significant and a recurring interaction in triplicate docking calculations, which is established between the R68 and bromine atom of compound **15** (Table S5).

3.3. Pharmacokinetic and toxicological properties

The calculated pharmacokinetic parameters (Table 3) show that the 5 selected compounds are candidates as fragment leads. The solubility (cLogS) for all compounds was found in an acceptable range (<4)⁶⁰. The cLogP parameter, which is directly related to a more favourable drug-likeness profile when ≤ 5 ^{61,62}, shows that all compounds meet this rule. They all have molecular weights ≤ 500 g/mol, which means that transportation and absorption are easier than heavy molecules⁶². Regarding the polar surface area criterium (PSA ≤ 140 Å² for oral bioavailability⁶² or 90 Å² for the cellular permeability⁶¹), all compounds showed acceptable results, with exception of compounds **1**, **4**, and **16** for cellular permeability. The results for donor sites (nOHNH) and hydrogen bonding acceptors (nOH), below 10 and 5, respectively, show that all compounds meet the rule for oral bioavailability⁶² and for crossing the blood-brain barrier (central nervous system, CNS)⁶¹. They all have rotatable bond ≤ 5 , which is related to the binding potency and penetration into the membrane⁶². Thus, the results showed that none of the studied compounds presented more than three violations to Lipinski's rule, suggesting they are suitable candidates for oral drugs.

The toxicity risk calculations search for substructures within the chemical structure being indicative of specific toxicity according to a reference database (Registry of Toxic Effects of Chemical Substances database – RTECS), which covers compounds of different toxicity classes^{49,63}. The absence of risky fragments suggests a low risk concerning the toxicity class under investigation⁶³. For these studies, the toxicity classes related to mutagenic, tumorigenic, or irritant effects or being associated with reproductive effects are considered. The results for all compounds showed they do not present any toxicological risks for those classes. It is important to emphasise that these results do not eliminate the need for traditional toxicological tests.

We evaluated the cytotoxicity of the compounds on Huh7 and A549 cells. Both cell lines were chosen because they are widely

used in studies of DENV infection and replication. The MTT assay was performed after 24 and 48 h of treatment with increasing concentrations of each compound (Figure 6, AJ). Cell lines maintained in culture medium with 0.5% DMSO were used as controls since this is the final DMSO concentration in the medium after the addition of the compounds. The viability results for cell treatment with each concentration of the compounds are expressed as a percentage related to cells treated with only DMSO, which did not significantly affect the cell viability. In general, the compounds were more toxic to Huh7 cells than to A549 cells. Compound **1** was very toxic to Huh7 cells even at low concentrations, leading to about 50% loss of viability at 30 μ M after 48 h (Figure 6(A)). On the other hand, for A549, the compound was toxic only at much higher concentrations, such as 400 μ M (Figure 6(B)). The most cytotoxic compound for both cells studied was compound **4**, with concentrations above 20 μ M being highly toxic (Figure 6(C–D)). On the other hand, compounds **12**, **15**, and **16** showed much more promising results (Figure 6(E–J)). Compounds **15** were toxic only at concentrations above 100 or 400 μ M to Huh7 or A549, respectively (Figure 6(G–H)), while compounds **12** and **16** were toxic to Huh7 only at concentrations above 400 μ M (Figure 6(E,I)), with even better results to A549 (Figure 6(F,J)). Compound **16** was non-toxic to A549 cells (Figure 6(J)) at all the concentrations tested and showed low cytotoxicity up to 100 μ M in Huh7 cells, with cell viability of 98% and 80% after 24 and 48 h treatment, respectively (Figure 6(I)). Therefore, among the tested compounds, compound **16** may be seen as the best candidate to explore a possible antiviral activity against DENV in future trials.

4. Conclusions

Here we presented a targeted screen of small aromatic compounds to the hydrophobic cleft ($\alpha 1$ - $\alpha 1'$ and $\alpha 2$ - $\alpha 2'$) of DENVC. The strategy was successful, enabling the description of new fragment leads that binds to the hydrophobic cleft, and this new series of compounds may be used as promising leads for dengue therapy. The advantages of these compounds include physical properties compatible with desirable pharmacokinetic parameters, such as low toxicity, simple synthetic procedure, and evidence of binding at a micromolar concentration to DENVC. Remarkably, STD-selected compounds elicited conformational changes upon DENVC binding. For compounds **1**, **4**, **12**, and **15**, the tryptophan residue (W69) is more solvent-exposed, possibly making the hydrophobic core looser, and for compound **16**, W69 is less solvent-exposed, hidden in a more rigid hydrophobic core. NMR-derived docking calculations suggest that the selected compounds are located in asymmetric binding sites formed by $\alpha 1$, $\alpha 2$, and $\alpha 3$ in the hydrophobic cleft, where W69 is at the centre. These studies should allow the development of antiviral analogs targeting the hydrophobic cleft of the DENVC and possibly blocking its interaction with lipid droplets.

Acknowledgements

The author IPC gratefully acknowledges the financial support by a postdoctoral fellowship from FAPERJ and the PROPe UNESP. The author LOO was a fellow of CAPES.

Disclosure statement

No potential conflict of interest was reported by the authors.

Funding

This work was supported by Fundação de Amparo à Pesquisa do Estado do Rio de Janeiro – FAPERJ, Brazil: Grant [255.940/2020, 202.279/2018, 239.229/2018, 202.945/2017, 201.316/2016, 210.361/2015, and 204.432/2014]. Conselho Nacional de Desenvolvimento Científico e Tecnológico – CNPq, Brazil: [439306/2018–3, 309564/2017–4, and 309028/2017–5. La Caixa Bank Foundation, Spain: LCF/PR/HR17/52150011].

ORCID

Ícaro P. Caruso  <http://orcid.org/0000-0003-4464-0520>

Fabio C. L. Almeida  <http://orcid.org/0000-0001-6046-7006>

References

- Guzman MG, Gubler DJ, Izquierdo A, et al. Dengue infection. *Nat Rev Dis Prim* 2016;2:1–25.
- Diamond MS, Pierson TC. Molecular insight into dengue virus pathogenesis and its implications for disease control. *Cell. Cell Press* 2015;162:488–92.
- Jones CT, Ma L, Burgner JW, et al. Flavivirus capsid is a dimeric alpha-helical protein. *J Virol* 2003;77:7143–9.
- Mukhopadhyay S, Kuhn RJ, Rossmann MG. A structural perspective of the flavivirus life cycle. *Nat Rev Microbiol* 2005;3:13–22.
- Neves-Martins TC, Mebus-Antunes NC, Caruso IP, et al. Unique structural features of flaviviruses' capsid proteins: new insights on structure-function relationship. *Curr Opin Virol* 2021;47:106–12.
- Morando MA, Barbosa GM, Cruz-Oliveira C, et al. Dynamics of zika virus capsid protein in solution: the properties and exposure of the hydrophobic cleft are controlled by the α -Helix 1 sequence. *Biochemistry* 2019;58:2488–98.
- Samsa MM, Mondotte JA, Iglesias NG, et al. Dengue virus capsid protein usurps lipid droplets for viral particle formation. Diamond MS, editor. *PLoS Pathog* 2009;5:e1000632.
- Martins IC, Gomes-Neto F, Faustino AF, et al. The disordered N-terminal region of dengue virus capsid protein contains a lipid-droplet-binding motif. *Biochem J* 2012;444:405–15.
- Faustino AF, Guerra GM, Huber RG, et al. Understanding dengue virus capsid protein disordered N-terminus and pep14-23-based inhibition. *ACS Chem Biol* 2015;10:517–26.
- Poh MK, Yip A, Zhang S, et al. A small molecule fusion inhibitor of dengue virus. *Antiviral Res* 2009;84:260–6.
- Steuer C, Gege C, Fischl W, et al. Synthesis and biological evaluation of α -ketoamides as inhibitors of the Dengue virus protease with antiviral activity in cell-culture. *Bioorg Med Chem* 2011;19:4067–74.
- Xie X, Wang Q-Y, Xu HY, et al. Inhibition of dengue virus by targeting viral NS4B protein. *J Virol* 2011;85:11183–95.
- Lim SP, Sonntag LS, Noble C, et al. Small molecule inhibitors that selectively block dengue virus methyltransferase. *J Biol Chem* 2011;286:6233–40.
- Chen Y-L, Yin Z, Duraiswamy J, et al. Inhibition of dengue virus RNA synthesis by an adenosine nucleoside. *Antimicrob Agents Chemother* 2010;54:2932–9.
- Niyomrattanakit P, Chen YL, Dong H, et al. Inhibition of dengue virus polymerase by blocking of the RNA tunnel. *J Virol* 2010;84:5678–86.
- Wang Q-Y, Kondreddi RR, Xie X, et al. A translation inhibitor that suppresses dengue virus in vitro and in vivo. *Antimicrob Agents Chemother* 2011;55:4072–80.
- Scaturro P, Trist IML, Paul D, et al. Characterization of the mode of action of a potent dengue virus capsid inhibitor. *J Virol* 2014;88:11540–55.
- Byrd CM, Dai D, Grosenbach DW, et al. A novel inhibitor of dengue virus replication that targets the capsid protein. *Antimicrob Agents Chemother* 2013;57:15–25.
- Xia H, Xie X, Zou J, et al. A cocrystal structure of dengue capsid protein in complex of inhibitor. *Proc Natl Acad Sci USA* 2020;117:17992–8001.
- Andreani A, Burnelli S, Granaiola M, et al. New antitumor Imidazo[2,1-b]Thiazole guanylhydrazones and analogues. *J Med Chem* 2008;51:809–16.
- Banday AH, Akram SMM, Shameem SA. Benzylidene pregnenolones and their oximes as potential anticancer agents: synthesis and biological evaluation. *Steroids* 2014;84:64–9.
- Harini ST, Kumar HV, Rangaswamy J, et al. Synthesis, antioxidant and antimicrobial activity of novel vanillin derived piperidin-4-one oxime esters: preponderant role of the phenyl ester substituents on the piperidin-4-one oxime core. *Bioorg Med Chem Lett* 2012;22:7588–92.
- Singh B, Maheshwari A, Dak G, et al. Studies of antimicrobial activities of some 4-thiazolidinone fused pyrimidines, [1,5]-benzodiazepines and their oxygen substituted hydroxylamine derivatives. *Indian J Pharm Sci* 2010;72:607–12.
- Lazić J, Ajdačić V, Vojnovic S, et al. Bis-guanylhydrazones as efficient anti-Candida compounds through DNA interaction. *Appl Microbiol Biotechnol* 2018;102:1889–901.
- Rossello A, Bertini S, Lapucci A, et al. Synthesis, antifungal activity, and molecular modeling studies of new inverted oxime ethers of oxiconazole. *J Med Chem* 2002;45:4903–12.
- Zhang L, Jiang CS, Gao LX, et al. Design, synthesis and in vitro activity of phidianidine B derivatives as novel PTP1B inhibitors with specific selectivity. *Bioorg Med Chem Lett* 2016;26:778–81.
- Shamroukh AH, Zaki MEA, Morsy EMH, et al. Synthesis of pyrazolo[4',3':5,6]pyrano[2,3-d]pyrimidine derivatives for anti-viral evaluation. *Arch Pharm* 2007;340:236–43.
- Degardin M, Wein S, Duckert J-F, et al. Development of the first oral bioprecursors of bis-alkylguanidine antimalarial drugs. *ChemMedChem* 2014;9:300–4.
- Papanastasiou I, Tsotinis A, Zoidis G, et al. Design and synthesis of *Trypanosoma brucei* active 1-alkyloxy and 1-benzoyloxyadamantano 2-guanylhydrazones. *ChemMedChem* 2009;4:1059–62.
- Mohassab AM, Hassan HA, Abdelhamid D, et al. Novel quinoline incorporating 1,2,4-triazole/oxime hybrids: synthesis, molecular docking, anti-inflammatory, COX inhibition, ulcerogenicity and histopathological investigations. *Bioorg Chem* 2017;75:242–59.
- Ottanà R, Maccari R, Barreca ML, et al. 5-Arylidene-2-imino-4-thiazolidinones: design and synthesis of novel anti-inflammatory agents. *Bioorg Med Chem* 2005;13:4243–52.
- Petronilho E da C, Rennó M do N, Castro NG, et al. Design, synthesis, and evaluation of guanylhydrazones as potential inhibitors or reactivators of acetylcholinesterase. *J Enzyme Inhib Med Chem* 2016;31:1069–78.
- Prasad RN, McKay AF. Acylation of guanidines and guanylhydrazones. *Can J Chem* 1967;45:2247–52.
- Amidi S, Esfahanizadeh M, Tabib K, et al. Rational design and synthesis of 1-(arylideneamino)-4-aryl-1H-imidazole-2-

- amine derivatives as antiplatelet agents. *ChemMedChem* 2017;12:962–71.
35. Bonomi P, Servant A, Resmini M. Modulation of imprinting efficiency in nanogels with catalytic activity in the Kemp elimination. *J Mol Recognit* 2012;25:352–60.
 36. Jiménez-Juárez R, Cruz-Chávez W, de Jesús-Ramírez N, et al. Synthesis and antimycobacterial activity of 2,5-disubstituted and 1,2,5-trisubstituted benzimidazoles. *Front Chem* 2020;8:433.
 37. Irfan I, Sawangjaroen N, Bhat AR, et al. New dioxazole derivatives: synthesis and effects on the growth of *Entamoeba histolytica* and *Giardia intestinalis*. *Eur J Med Chem* 2010;45:1648–53.
 38. Trefzger OS, Barbosa NV, Scapolatempo RL, et al. Design, synthesis, antileishmanial, and antifungal biological evaluation of novel 3,5-disubstituted isoxazole compounds based on 5-nitrofurans scaffolds. *Arch Pharm* 2020;353:1900241.
 39. Carvalho FAA, Carneiro FAA, Martins ICC, et al. Dengue virus capsid protein binding to hepatic lipid droplets (LD) is potassium ion dependent and is mediated by LD surface proteins. *J Virol* 2012;86:2096–108.
 40. Hwang TL, Shaka AJ. Water suppression that works. Excitation sculpting using arbitrary wave-forms and pulsed-field gradients. *J Magn Reson Ser A* 1995;112:275–9.
 41. Grzesiek S, Bax A. The importance of not saturating water in protein NMR. Application to sensitivity enhancement and NOE measurements. *J Am Chem Soc* 1993;115:12593–4.
 42. Kay L, Keifer P, Saarinen T. Pure absorption gradient enhanced heteronuclear single quantum correlation spectroscopy with improved sensitivity. *J Am Chem Soc* 1992;114:10663–5.
 43. Palmer AG, Cavanagh J, Wright PE, et al. Sensitivity improvement in proton-detected two-dimensional heteronuclear correlation NMR spectroscopy. *J Magn Reson* 1991;93:151–70.
 44. Schleucher J, Schwendinger M, Sattler M, et al. A general enhancement scheme in heteronuclear multidimensional NMR employing pulsed field gradients. *J Biomol NMR* 1994;4:301–6.
 45. Vranken WF, Boucher W, Stevens TJ, et al. The CCPN data model for NMR spectroscopy: development of a software pipeline. *Proteins Struct Funct Genet* 2005;59:687–96.
 46. Ma L, Jones CT, Groesch TD, et al. Solution structure of dengue virus capsid protein reveals another fold. *Proc Natl Acad Sci USA* 2004;101:3414–9.
 47. Markley JL, Ulrich AEEL, Berman AEHM, et al. BioMagResBank (BMRB) as a partner in the Worldwide Protein Data Bank (wwPDB): new policies affecting biomolecular NMR depositions. *J Biomol NMR* 2008;40:153–5.
 48. Caruso IP, Guimaraes GC, Machado VB, et al. Biophysical and dynamic characterization of fine-tuned binding of the human respiratory syncytial virus M2-1 core domain to long RNAs. *J Virol* 2020;94(23):e01505-20.
 49. Sander T, Freyss J, von Korff M, et al. DataWarrior: an open-source program for chemistry aware data visualization and analysis. *J Chem Inf Model* 2015;55:460–73.
 50. Frisch MJ, Trucks GW, Schlegel HB, et al. Gaussian 09. Wallingford, CT: Gaussian, Inc.; 2016.
 51. Sanner MF. Python: a programming language for software integration and development. *J Mol Graph Model* 1999;17:57–61.
 52. Trott O, Olson AJ. AutoDock Vina: improving the speed and accuracy of docking with a new scoring function, efficient optimization, and multithreading. *J Comput Chem* 2009;31:NA.
 53. Salentin S, Schreiber S, Haupt VJ, et al. PLIP: fully automated protein-ligand interaction profiler. *Nucleic Acids Res* 2015;43:W443–W447.
 54. Delano WL. The PyMOL molecular graphics system. San Carlos (CA): DeLano Scientific; 2002.
 55. Hunan Huateng Pharmaceutical Co. L. A kind of preparation method of bridged piperazine derivatives. Republic of China Patent. CN106810513A, filed October 1, 2017, and issued September 6, 2017.
 56. Dengke L, Xiaoli F, Ying L, et al. Preparation of 6,7-dihydro-4H-thieno[3,2-c]pyridine derivatives for treatment of depression. Republic of China Patent. CN 102503953, filed October 20, 2011, and issued June 20, 2012.
 57. Figueroa-Villar J, Tinoco L. Spin-lattice relaxation time in drug discovery and design. *Curr Top Med Chem* 2009;9:811–823.
 58. Figueiredo IM, Marsaioli AJ. Mapeamento das interações proteína-ligante através de técnicas de RMN de ^1H utilizando detecção do ligante. *Quim Nova* 2007;30:1597–1605.
 59. Weber G. Fluorescence-polarization spectrum and electronic-energy transfer in tyrosine, tryptophan and related compounds. *Biochem J* 1960;75:335–345.
 60. Meanwell NA. Improving drug candidates by design: a focus on physicochemical properties as a means of improving compound disposition and safety. *Chem Res Toxicol* 2011;24:1420–1456.
 61. Pajouhesh H, Lenz GR. Medicinal chemical properties of successful central nervous system drugs. *NeuroRX* 2005;2:541–553.
 62. Lipinski CA. Lead- and drug-like compounds: the rule-of-five revolution. *Drug Discov Today Technol* 2004;1:337–341.
 63. von Korff M, Sander T. Toxicity-indicating structural patterns. *J Chem Inf Model* 2006;46:536–544.